Measurement: Sensors 41 (2025) 101971

Contents lists available at ScienceDirect

Measurement: Sensors

journal homepage: www.sciencedirect.com/journal/measurement-sensors

Two-step compensation via rotational stepping error fitting for precise azimuth measurement with electronic compass

Jinshuo Ma [a,1], Ningfeng Zhang [a,1], Tao Zhang [b], Jinyu Ma [a], Jian Li [a], Xinjing Huang [a,*]

[a] State Key Laboratory of Precision Measurement Technology and Instruments, Tianjin University, Tianjin, China
[b] Tianjin Institute of Metrological Supervision and Testing, Tianjin, China

ARTICLE INFO

Keywords:
Electronic compass
Rotational stepping
Error fitting
Azimuth compensation

ABSTRACT

Marine buoys commonly employ electronic compasses to measure their azimuth angles under the requirements for low power consumption and high precision. After installation on buoys, geomagnetic electronic compasses often suffer from measurement errors in azimuth angles due to manufacturing errors and magnetic interference from the buoy structure. This paper presents a two-step compensation method for azimuth measurement errors of electronic compass based on rotational step error fitting. In the first step, before installation on the buoy, the magnetometer of the electronic compass is calibrated using the ellipsoidal fitting method, which requires arbitrary rotation of the lightweight compass around multiple different axes. In the second step, after mounting the electronic compass inside the buoy, stepwise rotations are performed to collect azimuth measurement errors at various angles. The least squares method is then applied to fit the developed error function relative to rotation angle to generate compensation values for various azimuths, which are used for secondary error compensation. Experimental results demonstrate that using azimuth angles calculated by high-precision satellite positioning devices as absolute reference values, the measurement accuracy of azimuth angles reaches 0.6° after applying the proposed compensation method to the electronic compass. This approach avoids the use of three-dimensional rotation operations or large Helmholtz coils and is therefore simple and suitable for field operation.

1. Introduction

Marine buoys require accurate azimuth measurements while monitoring wave characteristics [1] and meteorological parameters [2] to calculate wave direction, ocean current direction, and wind direction. Current methods for buoy azimuth measurement include satellite positioning, gyroscopic techniques, and electronic compasses. Satellite positioning involves measuring the latitude and longitude of two points on a buoy using high-precision Global Navigation Satellite System (GNSS) receivers to calculate the azimuth angle between the two points [3]. The measurement accuracy increases with distance between the two points; however, buoys' limited size precludes the installation of large receiver pair. The gyroscopic approach utilizes laser gyroscopes or MEMS gyroscopes to measure three-axis angular velocity, which is then integrated to obtain the buoy's azimuth angle. This method requires periodic calibration to maintain accuracy and is suitable only for short-term measurements [4], rendering it impractical for buoys requiring long-term, high-precision azimuth measurements. Electronic compasses calculate azimuth angles using measurements from magnetometers and accelerometers, offering advantages such as small size, low power consumption, and absence of cumulative errors [5], making them most suitable for long-term deployment on buoys. However, due to manufacturing process limitations, magnetometers inherently exhibit zero-bias errors, sensitivity errors, and non-orthogonality errors, while also being susceptible to hard and soft magnetic interferences from the carrier platform. These factors contribute to errors in azimuth measurements obtained from electronic compasses. Therefore, compensation and calibration of electronic compasses are necessary to obtain accurate azimuth information.

There are mainly five methods for correcting electronic compasses: high-precision sensor reference method, Helmholtz coil method, dual satellite positioning method, ellipsoid fitting method, and non-magnetic turntable method.

The high-precision sensor reference method involves assembling a high-precision reference sensor with the electronic compass under test, utilizing output data from the former to calibrate errors in the latter.

* Corresponding author.
E-mail address: huangxinjing@tju.edu.cn (X. Huang).
[1] Jinshuo Ma and Ningfeng Zhang contributed equally to the work.

https://doi.org/10.1016/j.measen.2025.101971
Received 13 June 2025; Received in revised form 14 August 2025; Accepted 9 September 2025
Available online 10 September 2025

High-precision reference sensors include high-precision compasses [6], high-precision magnetometers [7] and high-precision gyroscopes [8]. The former directly compares outputs, while the latter correlates the magnetometer's magnetic field variation rate with gyroscope angular velocity, employing least squares method to solve for error parameters and achieve electronic compass calibration. Additionally, researchers have employed gyroscopes to assist in magnetometer calibration for electronic compasses [9]. This approach transforms magnetometer measurements into an inertial coordinate system using trial parameters to be calibrated and attitude matrices calculated by the gyroscope. The transformed measurements are then matched with a constant geomagnetic field vector. By minimizing the errors in this matching process across all calibration time points, calibration parameters can be estimated, thereby completing magnetometer calibration.

The Helmholtz coil method introduces identical currents into two circular coils with equal radius, positioned coaxially at a distance equal to the coil radius. The magnetic fields generated by the two coils superimpose, creating a uniform magnetic field in the central region [10]. Through the configuration of three orthogonal pairs of Helmholtz coils, a uniform magnetic field with precisely adjustable magnitude and direction can be generated. This method places the electronic compass in the central region of the coils and achieves calibration by controlling the currents in the three coil pairs to alter the magnetic field's magnitude and direction. The approach eliminates the need for physical rotation of the electronic compass, making it particularly suitable for large, rotation-restricted carriers such as geomagnetic satellites [11], geomagnetic vector measurement systems [12], and hydrophone arrays [13]. This method is limited by the relatively small region of uniform magnetic field generated in the center of Helmholtz coils. When applied to calibrating buoys equipped with electronic compasses, issues arise regarding excessively large coil dimensions and prohibitively high costs.

The dual satellite positioning method involves mounting the electronic compass to be calibrated on a satellite positioning device, and the absolute azimuth angle is determined using the geographic coordinate outputs of the two positioning devices, thereby enabling the angular calibration of the electronic compass. This approach eliminates the necessity of collecting spatial magnetic field data at various rotational attitudes. Le Menn et al. [14] addressed the calibration issue of electronic compasses installed inside ocean current meters by mounting the electronic compass on a rotating platform equipped with GPS. The external azimuth reference was calculated based on the reference GPS, which subsequently facilitated the correction of electronic compass output values. The platform was further improved [15] with the addition of a tilting mechanism that enabled the calibration of inclination sensors. This method presents a limitation in that the positioning equipment required for calibration is prohibitively expensive.

The ellipsoid fitting method represents the predominant approach for magnetometer calibration. This technique involves the approximately uniform collection of spatial magnetic field data from the magnetometer at various attitudes. It exploits the characteristic ellipsoidal distribution of magnetic data in the presence of measurement errors and magnetic interference. By fitting an ellipsoid and obtaining calibration parameters, the magnetic data is corrected to exhibit a spherical distribution, thereby eliminating magnetometer measurement errors and carrier magnetic interference. Representative works include: Renaudin et al. [16], who thoroughly proposed and elaborated on the ellipsoid fitting method, Yang et al. [17], who suggested improving the ellipsoid fitting method through truncated singular value decomposition, and Kiani et al. [18], who introduced statistical bias and optimized normalization constraints, improving the calibration accuracy of the ellipsoid fitting method. This method has been applied to magnetometer calibration in rotating projectiles [19], combined with accelerometer multi-position calibration methods for electronic compass correction [20], and utilized in azimuth error correction of vector field measurement systems [21]. This approach solely addresses the calibration of individual sensors and fails to ensure three-axis alignment between two sensors.

The non-magnetic turntable method involves mounting the electronic compass on a non-magnetic turntable, utilizing the turntable's capability for arbitrary rotation and provision of reference angles to achieve electronic compass calibration. This method enables both ellipsoid fitting calibration of the magnetometer and azimuth correction of the electronic compass according to reference angles. Liu et al. [22] collected magnetic data from the magnetometer at various attitudes using a non-magnetic turntable and completed the electronic compass magnetometer calibration through the ellipsoid fitting method. Le Menn et al. [23] utilized a non-magnetic platform to collect measurement errors of marine electronic compasses at different azimuth angles and derived error expressions [24] to complete electronic compass calibration. Chu et al. [25] measured the deviation angles between the magnetometer and electronic compass measurement coordinate system axes using a non-magnetic turntable to derive the calibration matrix for the electronic compass magnetometer. Additionally, the non-magnetic turntable method facilitates three-axis alignment between two sensors. Zhu et al. [26] and Liu et al. [27] developed calibration algorithms based on non-magnetic turntables, deriving the three-step methods of ellipsoid fitting-dot product invariance-optimal synthetic vector and ellipsoid fitting-platform fitting-dot product invariance, respectively, for joint calibration of magnetometers and accelerometers in electronic compasses. A limitation of this method lies in the typically small size of non-magnetic turntables, which precludes the calibration of buoys equipped with electronic compasses.

This paper addresses the calibration issue of electronic compasses inside buoys and proposes a joint two-step compensation method that considers buoy size limitations and conventional calibration approaches: First, before installation in the buoy, the electronic compass magnetometer undergoes calibration using the ellipsoid fitting method, which requires arbitrary rotation of the electronic compass around multiple different axes. Second, after installation of the electronic compass inside the buoy, rotational stepping secondary compensation is performed to improve azimuth measurement accuracy, requiring only one complete rotation of the buoy around the vertical axis. The subsequent content of this paper is organized as follows: Section 2 presents the working principles of electronic compasses, conventional manufacturing error compensation methods, and the fundamental principles of rotational stepping secondary compensation for azimuth error. Section 3 details the validation methodology, encompassing electronic compass hardware design, manufacturing error compensation, and verification of the rotational stepping secondary compensation scheme. Section 4 describes the application of this method to simulated buoys and presents experimental validation of directional accuracy after secondary compensation using dual satellite positioning devices. Section 5 provides conclusions and summary.

2. Methodology

2.1. Electronic compass operating principles and ellipsoid fitting method

In the electronic compass coordinate system (S), the x-axis points forward, the y-axis points to the left, and the z-axis points upward. In the navigation coordinate system (S_g), the x_g-axis points northward along the horizontal plane, the y_g-axis points westward along the horizontal plane, and the z_g-axis points vertically upward, as illustrated in Fig. 1.

The angle between magnetic north N_M and geographic north N_G is defined as the magnetic declination β. If **OB** represents the magnetic induction intensity vector at a specific point in space, it can be decomposed into three axial components (B_{xg}, B_{yg}, B_{zg})in the S_g coordinate system, as shown in Fig. 1. $\mathbf{OB_L}$ is the projection of **OB** onto the x_gOy_g plane. The magnetic azimuth angle φ_1 is expressed as:

$$\varphi_1 = \arctan\left(B_{yg}/B_{xg}\right) \tag{1}$$

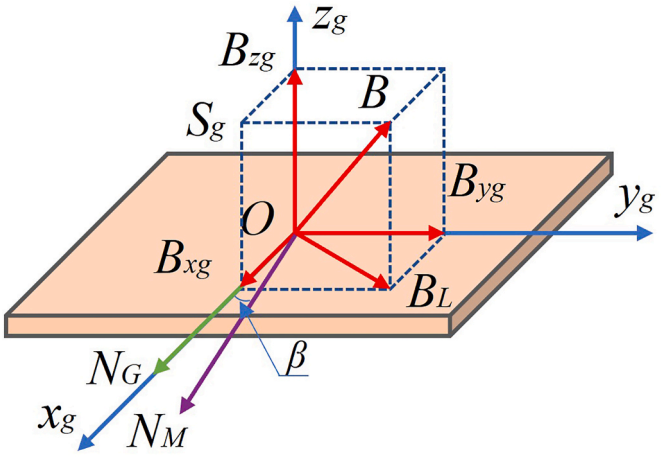

Fig. 1. Schematic diagram of the navigation coordinate system S_g.

where B_{xg} and B_{yg} represent the components of **OB** along the x_g-axis and y_g-axis, respectively.

When the S and S_g coordinate systems coincide, the components of **OB** along the x-axis and y-axis are identical to B_{xg} and B_{yg}, respectively, yielding B_{xg}=B_x and B_{yg}=B_y. Consequently, (1) can be directly applied to calculate the magnetic azimuth angle.

When the S and S_g coordinate systems do not coincide, the rotational relationship between them is characterized by the pitch angle θ and roll angle γ. As illustrated in Fig. 2, this rotation can be described as a clockwise rotation of S_g around the y-axis by angle θ to reach S', followed by a clockwise rotation around the x-axis by angle γ to reach S. The transformation equation between the navigation coordinate system S_g and the electronic compass coordinate system S can be derived as [28]:

$$\begin{bmatrix} B_x \\ B_y \\ B_z \end{bmatrix} = \begin{bmatrix} 1 & 0 & 0 \\ 0 & \cos\gamma & -\sin\gamma \\ 0 & \sin\gamma & \cos\gamma \end{bmatrix} \begin{bmatrix} \cos\theta & 0 & \sin\theta \\ 0 & 1 & 0 \\ -\sin\theta & 0 & \cos\theta \end{bmatrix} \begin{bmatrix} B_{xg} \\ B_{yg} \\ B_{zg} \end{bmatrix} \tag{2}$$

Substituting (2) into (1) completes the tilt compensation, resulting in the magnetic azimuth angle φ_2:

$$\varphi_2 = \arctan\left(\frac{B_y\cos\gamma + B_z\sin\gamma}{B_x\cos\theta + B_y\sin\theta\sin\gamma - B_z\sin\theta\cos\theta}\right) \tag{3}$$

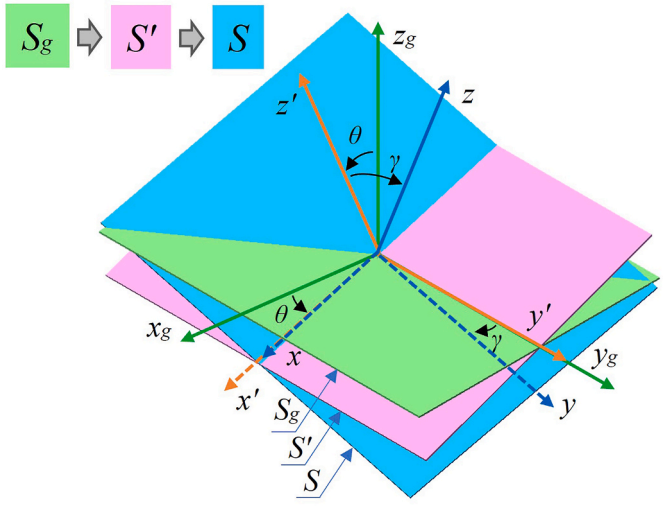

Fig. 2. Schematic diagram of the rotational relationship between coordinate systems S and S_g.

The pitch angle θ and roll angle γ can be calculated from the accelerometer data of the electronic compass, specifically utilizing the gravitational components (f_x, f_y, f_z) along the three axes of the S coordinate system [20]:

$$\begin{aligned} \theta &= \cot\left(\frac{f_x}{\sqrt{f_y^2+f_z^2}}\right) \\ \gamma &= \cot\left(\frac{f_y}{\sqrt{f_x^2+f_z^2}}\right) \end{aligned} \tag{4}$$

The calculated magnetic azimuth angle encompasses both the azimuth angle ϕ and the magnetic declination β. Therefore, to determine the object's azimuth angle ϕ relative to geographic north, the magnetic declination β must be subtracted:

$$\varphi = \varphi_2 - \beta \tag{5}$$

Manufacturing errors in magnetometers include tri-axial sensitivity errors, tri-axial zero-point offsets, tri-axial non-orthogonality errors, as well as soft and hard magnetic interferences from other components of the electronic compass [29]. These interferences can be modeled as:

$$\mathbf{B_m} = \mathbf{SN}(\mathbf{R_{si}B} + \mathbf{b_{hi}}) + \mathbf{b_{so}} + \boldsymbol{\varepsilon} = \mathbf{MB} + \mathbf{b} + \boldsymbol{\varepsilon} \tag{6}$$

In this model, $\mathbf{B_m}$ represents the magnetometer output under manufacturing errors. **B** denotes the ideal magnetic induction intensity vector at the magnetometer's position. Matrix **S** represents the tri-axial sensitivity errors as a 3 × 3 diagonal matrix. Vector **N** represents the tri-axial non-orthogonality errors. Vector $\mathbf{b_{so}}$ represents the tri-axial zero-point offsets. Vector $\mathbf{b_{hi}}$ represents the hard magnetic interferences affecting the tri-axial magnetometer. Vector $\mathbf{R_{si}}$ represents the soft magnetic interferences affecting the tri-axial magnetometer, and ε denotes the noise interference of the tri-axial magnetometer, primarily originating from equipment noise. The error model can be simplified by unifying different error representations. **M** is a 3 × 3 matrix encompassing tri-axial sensitivity errors, tri-axial non-orthogonality errors, and soft magnetic interferences. **b** is a column vector encompassing tri-axial zero-point offsets and hard magnetic interferences.

The ellipsoid fitting method can be employed to correct manufacturing errors in magnetometers. As this method is well-established, the corresponding derivation process is abbreviated in this paper.

Based on (6), the following transformation can be derived:

$$\mathbf{B} = \mathbf{M}^{-1}(\mathbf{B_m} - \mathbf{b}) \tag{7}$$

Given the characteristics of Earth's magnetic field, the magnitude and direction of the magnetic field at the same location during the same time period remain constant, leading to:

$$|\mathbf{B}|^2 = (\mathbf{B_m} - \mathbf{b})^{\mathrm{T}}(\mathbf{M}^{-1})^{\mathrm{T}}\mathbf{M}^{-1}(\mathbf{B_m} - \mathbf{b}) \tag{8}$$

By establishing a three-dimensional matrix **A**, which can be determined as a symmetric matrix based on its creation conditions, the elements of matrix A can be postulated as:

$$\mathbf{A} = (\mathbf{M}^{-1})^{\mathrm{T}}\mathbf{M}^{-1} = \begin{bmatrix} a & b/2 & d/2 \\ b/2 & c & e/2 \\ d/2 & e/2 & f \end{bmatrix} \tag{9}$$

Substituting (9) into (8) yields:

$$|\mathbf{B}|^2 = (\mathbf{B_m} - \mathbf{b})^{\mathrm{T}}\mathbf{A}(\mathbf{B_m} - \mathbf{b}) \tag{10}$$

Based on the characteristic ellipsoidal distribution of measured tri-axial magnetic data in the three-dimensional coordinate system, (10) can be transformed and simplified into a quadratic surface expression:

$$F = \mathbf{X}\cdot\boldsymbol{\alpha} = aB_{mx}^2 + bB_{mx}B_{my} + cB_{my}^2 + dB_{mx}B_{mz} + eB_{my} + fB_{mz}^2 + pB_{mx} + qB_{my} + rB_{mz} + s \tag{11}$$

$$\mathbf{X} = \begin{bmatrix} B_{mx}^2 & B_{mx}B_{my} & B_{my}^2 & B_{mx}B_{mz} & B_{my} & B_{mz}^2 & B_{mx} & B_{my} & B_{mz} & 1 \end{bmatrix}$$
$$\boldsymbol{\alpha} = [\, a \;\; b \;\; c \;\; d \;\; e \;\; f \;\; p \;\; q \;\; r \;\; s \,]^{\mathrm{T}} \tag{12}$$

Based on (10) and (11), the expression for column vector $\mathbf{b}$ can be derived:

$$\mathbf{b} = -\frac{1}{2}\mathbf{A}^{-1}\begin{bmatrix} p \\ q \\ r \end{bmatrix} \tag{13}$$

The electronic compass collects N sets of tri-axial magnetic data at the same position by changing its orientation over a period of time. The sum of squared distances from each set of tri-axial magnetic data points to the ellipsoidal surface is:

$$E = \sum_{i=1}^{N} F^2 = |\mathbf{D}\boldsymbol{\alpha}|^2 = \boldsymbol{\alpha}^{\mathrm{T}}\mathbf{D}^{\mathrm{T}}\mathbf{D}\boldsymbol{\alpha}$$
$$\mathbf{D} = [\, \mathbf{X_1} \quad \mathbf{X_2} \quad \cdots \quad \mathbf{X_N} \,]^{\mathrm{T}} \tag{14}$$

Since (11) is a general expression for quadratic surfaces capable of representing various quadratic surfaces including ellipsoidal surfaces. Grammalidis and Strintzis [30] proposed that the three-dimensional matrix $\mathbf{A}$ must be positive definite or negative definite and satisfy the following two constraints to fit the ellipsoidal surface parameter vector $\boldsymbol{\alpha}$:

$$\begin{aligned} &i.\boldsymbol{\alpha}^{\mathrm{T}}\mathbf{C}\boldsymbol{\alpha} > \mathbf{0} \\ &ii.(a+c)det(\mathbf{A}) > 0 \end{aligned} \tag{15}$$

where $\mathbf{C} = \begin{bmatrix} \mathbf{C_1} & \mathbf{C_2} \\ \mathbf{C_3} & \mathbf{C_4} \end{bmatrix}$, $\mathbf{C_1} = \begin{bmatrix} 0 & 0 & 2 \\ 0 & -1 & 0 \\ 2 & 0 & 0 \end{bmatrix}$, $\mathbf{C_2} = \mathbf{0}_{3\times7}$, $\mathbf{C_2} = \mathbf{0}_{7\times3}$, $\mathbf{C_2} = \mathbf{0}_{3\times3}$.

Fitzgibbon et al. [31] introduced the Lagrange Multiplier λ and demonstrated that the eigenvector corresponding to the non-negative eigenvalue of (16) is the optimal solution for $\boldsymbol{\alpha}$:

$$\mathbf{D}^{\mathrm{T}}\mathbf{D}\boldsymbol{\alpha} = \lambda\mathbf{C}\boldsymbol{\alpha} \tag{16}$$

Transforming (16) into:

$$(\mathbf{D}^{\mathrm{T}}\mathbf{D})^{-1}\mathbf{C}\boldsymbol{\alpha} = \boldsymbol{\alpha}/\lambda \tag{17}$$

The optimal solution for $\boldsymbol{\alpha}$ can be obtained by solving for the eigenvector corresponding to the non-negative eigenvalue of (17). Matrix $\mathbf{A}$ can then be determined using the elements of $\boldsymbol{\alpha}$ from (12) in (9), and vector $\mathbf{b}$ can be determined using (13).

Based on the preceding analysis, the complete ellipsoid fitting method for electronic compasses can be divided into the following steps:

1. Construct matrix $\mathbf{D}$ using a large volume of magnetic data collected by the electronic compass in various orientations, according to (12) and (14).
2. Construct matrix $(\mathbf{D}^{\mathrm{T}}\mathbf{D})^{-1}\mathbf{C}$ using matrices $\mathbf{D}$ and $\mathbf{C}$, according to Equation (17).
3. Solve for the non-negative eigenvalue of matrix $(\mathbf{D}^{\mathrm{T}}\mathbf{D})^{-1}\mathbf{C}$, where the corresponding eigenvector is the ellipsoidal parameter vector.
4. Construct matrix $\mathbf{A}$ using the ellipsoidal parameter vector $\boldsymbol{\alpha}$ according to (9) and (12), then determine vector $\mathbf{b}$ using (13).
5. Decompose matrix $\mathbf{A}$ according to (9) to obtain matrix $\mathbf{M}^{-1}$.
6. Calculate the corrected magnetic data using (7).

2.2. Sources of error

After completing the first-step correction using the ellipsoid fitting method for the tri-axial magnetometer, the output data transforms from an ellipsoidal distribution of magnetic data to a spherical distribution. This transformation indicates that sensitivity errors, zero-point offsets, non-orthogonality errors, hard magnetic interferences, and soft magnetic interferences of the magnetic sensor have been compensated. However, errors still persist when measuring azimuth angles after installing the electronic compass onto a buoy. These errors primarily consist of two components: first, rotational errors that remain uncorrected after ellipsoidal calibration; second, changes in magnetic interference experienced by the electronic compass due to the influence of other magnetic objects on the buoy after installation. These two types of errors are elaborated below.

The first source of error arises during the ellipsoid fitting process, where decomposing matrix $\mathbf{A}$ to obtain matrix $\mathbf{M}^{-1}$ introduces an additional orthogonal matrix $\mathbf{R}$, resulting in infinite solutions. This decomposition process can be represented as [32]:

$$\mathbf{A} = \left(\mathbf{M}^{-1}\right)^{\mathrm{T}}\mathbf{M}^{-1} = \left((\mathbf{RM})^{-1}\right)^{\mathrm{T}}(\mathbf{RM})^{-1} \tag{18}$$

where $\mathbf{R}$ is an arbitrary orthogonal matrix. This orthogonal matrix $\mathbf{R}$ implies that the magnetic sensor coordinate system after ellipsoid fitting correction can be rotated in any direction, and the rotated coordinate system also constitutes a solution to the ellipsoid fitting method. This issue creates rotational errors between the magnetometer coordinate system and the buoy coordinate system, which can be expressed as:

$$\mathbf{B_e} = \mathbf{RM}^{-1}(\mathbf{B_m} - \mathbf{b}) \tag{19}$$

where $\mathbf{B_e}$ represents the tri-axial measurements of the magnetometer after ellipsoid fitting correction.

The second source of error occurs when the electronic compass is installed inside the buoy, causing changes in the surrounding magnetic interference environment. Consequently, the relationship between the tri-axial measurements of the magnetometer installed inside the buoy and the tri-axial measurements after ellipsoid fitting correction can be expressed as [33]:

$$\mathbf{B_b} = \mathbf{C_{soft}}\mathbf{B_e} + \mathbf{b_{hard}} \tag{20}$$

where $\mathbf{B_b}$ represents the tri-axial measurements of the magnetometer installed inside the buoy, and $\mathbf{C_{soft}}$ and $\mathbf{b_{hard}}$ represent the soft magnetic interference matrix and hard magnetic interference vector generated by other devices affecting the magnetometer, respectively.

Based on the preceding analysis and (7), (19), and (20), the relationship between the tri-axial measurements $\mathbf{B_b}$ of the magnetometer installed inside the buoy and the ideal magnetic induction intensity vector $\mathbf{B}$ at the magnetometer's position can be derived as:

$$\mathbf{B_b} = \mathbf{C_{soft}}\mathbf{RB} + \mathbf{b_{hard}} \tag{21}$$

However, due to size constraints of the buoy, the electronic compass installed inside cannot undergo further ellipsoid fitting to compensate for these errors, necessitating the implementation of alternative methods.

2.3. Secondary compensation method based rotational stepping error fitting

Inspired by the maritime compass calibration method [23], we propose a secondary azimuth angle compensation for buoys using the rotational stepping error fitting compensation method as the second step, building upon the primary correction achieved through ellipsoid fitting. According to (21), the relationship between $\mathbf{B_b}$ and $\mathbf{B}$ can be represented as follows:

$$\begin{bmatrix} B_{bx} \\ B_{by} \\ B_{bz} \end{bmatrix} = \begin{bmatrix} a & b & c \\ d & e & f \\ g & h & k \end{bmatrix} \begin{bmatrix} B_x \\ B_y \\ B_z \end{bmatrix} + \begin{bmatrix} P \\ Q \\ R \end{bmatrix} \tag{22}$$

Assuming the angle between the buoy and magnetic north is denoted as ε, and the magnetic north angle calculated from the electronic compass data after ellipsoidal fitting is ε', the error between the electronic compass and the buoy can be expressed as δ, where $\delta = \varepsilon - \varepsilon'$. The horizontal component of the Earth's magnetic field can be represented as $H_{xy} = \sqrt{B_x^2 + B_y^2}$, while the horizontal component of the composite magnetic field of the Earth and buoy can be represented as $H_{xy}{}' = \sqrt{B_{cx}^2 + B_{cy}^2}$. The inclination angle of the Earth's magnetic field is denoted as ξ. Consequently, the following relationship is established:

$$\begin{aligned} B_x &= H\cos\varepsilon \\ B_y &= -H\sin\varepsilon \\ B_z &= H\tan\xi \\ B_{cx} &= H'\cos\varepsilon' \\ B_{cy} &= -H'\sin\varepsilon' \end{aligned} \tag{23}$$

Substituting (23) into equation (22) yields:

$$H'\cos\varepsilon = (1+a)H\cos\varepsilon - bH\sin\varepsilon + cH\tan\xi + P \tag{24}$$

$$-H'\sin\varepsilon = (-\sin\varepsilon + d\cos\varepsilon)H - eH\sin\varepsilon + fH\tan\xi + Q \tag{25}$$

Let $\psi = 1 + (a+e)/2$, by performing calculations on (24) and (25), the following result is obtained:

$$\tan\delta = \frac{A + B\sin\varepsilon + C\cos\varepsilon + D\sin 2\varepsilon + E\cos 2\varepsilon}{1 + B\cos\varepsilon - C\sin\varepsilon + D\cos 2\varepsilon - E\sin 2\varepsilon} \tag{26}$$

where $A = (d-b)/2\psi$, $B = (c\tan\xi + P/H)/\psi$, $C = (f\tan\xi + Q/H)/\psi$, $D = (a-e)/2\psi$, $E = (b+d)/2\psi$.

In practice, only the azimuth angle ε' calculated by the electronic compass can be obtained. Therefore, $\varepsilon' + \delta$ is used to substitute for ε, and $\tan\delta$ is represented by $\sin\delta/\cos\delta$. After simplification, the following expression is derived:

$$\sin\delta = \frac{A\cos\delta + B\sin\varepsilon' + C\cos\varepsilon' + D\sin 2\varepsilon' + E\cos 2\varepsilon'}{1 - D\cos 2\varepsilon' + E\sin 2\varepsilon'} \tag{27}$$

For the deviation δ, $\sin\delta$ can be approximated as δ and $\cos\delta$ as 1. This approximation is valid when δ is less than 15° [24], which necessitates the preliminary calibration of the magnetic sensor. Subsequently, the denominator is expanded as a Fourier series of $2\varepsilon'$, resulting in the following infinite series:

$$\begin{aligned} f(\varepsilon') \quad &= A' + B'\sin\varepsilon' + C'\cos\varepsilon' + D'\sin 2\varepsilon' + E'\cos 2\varepsilon' \\ &\quad + F'\sin 3\varepsilon' + G'\cos 3\varepsilon' + \cdots \end{aligned} \tag{28}$$

where $A', B', C', D', E', F', G', \cdots$ are undetermined coefficients. Thus, an approximate expression for the azimuth angle deviation is established. In practical implementation, the azimuth angles and error data measured by the electronic compass can be collected to determine the error distribution pattern. Based on this pattern, (28) can be truncated accordingly, and appropriate undetermined coefficients can be calculated.

To enhance the accuracy of the azimuth angle deviation expression, the least squares method can be employed to calculate the error compensation coefficients. For the azimuth angle range of 0°–360°, σ sets of interval points can be selected with intervals of $360°/\sigma$. Based on the determined number of points, experiments can be conducted to obtain σ sets of data. Assuming the azimuth angle error distribution pattern is determined to be second-order, the collected σ sets of data can be written in matrix form as [34]:

$$\mathbf{J} = \mathbf{PQ} \tag{29}$$

where:

$$\mathbf{J} = \begin{bmatrix} \delta_1 \\ \vdots \\ \delta_\sigma \end{bmatrix} = \begin{bmatrix} \varepsilon_1{}' - 360°/\sigma\cdot 0 \\ \vdots \\ \varepsilon_\sigma{}' - 360°/\sigma\cdot(\sigma-1) \end{bmatrix}$$

$$\mathbf{P} = \begin{bmatrix} 1 & \sin\varepsilon_1{}' & \cos\varepsilon_1{}' & \sin 2\varepsilon_1{}' & \cos 2\varepsilon_1{}' \\ 1 & \sin\varepsilon_2{}' & \cos\varepsilon_2{}' & \sin 2\varepsilon_2{}' & \cos 2\varepsilon_2{}' \\ 1 & \sin\varepsilon_3{}' & \cos\varepsilon_3{}' & \sin 2\varepsilon_3{}' & \cos 2\varepsilon_3{}' \\ \vdots & \vdots & \vdots & \vdots & \vdots \\ 1 & \sin\varepsilon_\sigma{}' & \cos\varepsilon_\sigma{}' & \sin 2\varepsilon_\sigma{}' & \cos 2\varepsilon_\sigma{}' \end{bmatrix} \tag{30}$$

$$\mathbf{Q} = \begin{bmatrix} A' \\ \vdots \\ E' \end{bmatrix}$$

By applying the least squares method, the compensation parameter vector $\mathbf{Q}$ can be solved according to equation (29):

$$\mathbf{Q} = \left(\mathbf{P}^{\mathbf{T}}\mathbf{P}\right)^{-1}\mathbf{P}^{\mathbf{T}}\mathbf{J} \tag{31}$$

The solved compensation parameter vector $\mathbf{Q}$ can be substituted into (28) to obtain an accurate expression for the azimuth angle error. The parameter ζ is defined to represent the deviation between the azimuth angle fitting function and the collected azimuth angle data, expressed as $\zeta = \delta - f(\varepsilon')$. The parameter ζ_m is defined to characterize the deviation between the compensated azimuth angle and the true azimuth angle value. These variables, ζ and ζ_m, are employed to describe the accuracy of the fitting function and the azimuth angle accuracy after the completion of two-stage compensation, respectively.

3. Experimental design and analysis

3.1. Electronic compass hardware design

This study employed Honeywell's HMC1001 and HMC1002 magnetoresistive chips as magnetic sensors and ADI's ADXL345 chip as an accelerometer to construct a three-dimensional electronic compass. The HMC1001 and HMC1002 feature high resolution and linearity with a measurement range of ±2 G, enabling effective measurement of geomagnetic field strength. The ADXL345 chip is characterized by its small size and high precision. The three-dimensional electronic compass designed in this study converts magnetic signals into voltage signals, which are amplified by AD623, collected by ADS1274, and subsequently sent to a microprocessor for signal processing. The overall design scheme is illustrated in Fig. 3.

The electronic compass underwent ellipsoid fitting calibration to determine the manufacturing error compensation parameters of the magnetic sensors. The entire electronic compass was thoroughly rotated to collect and store magnetic data. The collected raw magnetic data was plotted in three-dimensional space, with the distribution shown as red points in Fig. 4. The three axes in the figure represent the three magnetic components B_x, B_y, and B_z measured in the electronic compass coordinate system. It is evident that the red points are distributed on an ellipsoid whose center is not at the origin and whose shape approximates a sphere.

The collected raw magnetic data was substituted into the ellipsoid fitting correction algorithm. The resulting correction parameters and original data were then input into equation (7) to obtain the calibrated

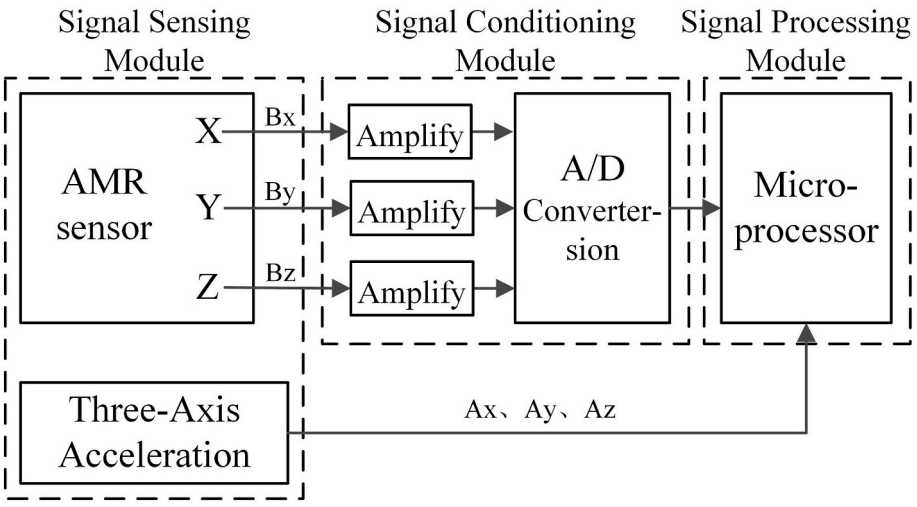

Fig. 3. Block diagram of the electronic compass design.

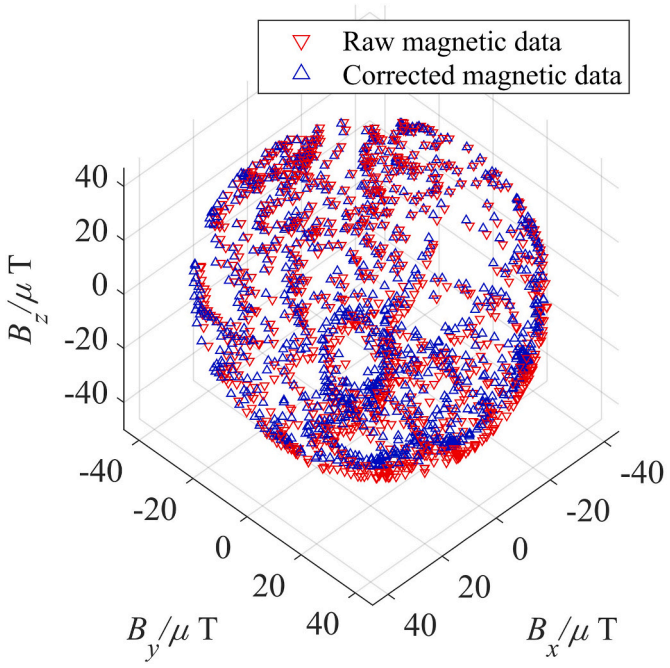

Fig. 4. Three-dimensional spatial distribution of raw magnetic data and calibrated magnetic data.

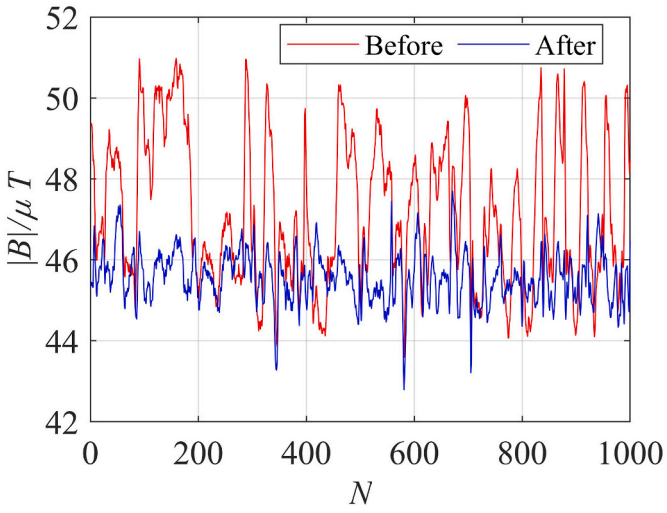

Fig. 5. Comparison of magnetometer data before and after ellipsoidal calibration.

data. The calibrated data was similarly plotted in three-dimensional space, as represented by the blue points in Fig. 4. It can be observed that the calibration process transforms the ellipsoid into a sphere centered at the origin. The magnetometer magnitude values $|B|$ before and after calibration were calculated separately for comparison, with the results illustrated in Fig. 5.

Fig. 5 depicts the magnitude values before and after calibration, where the horizontal axis represents the magnetic data sampling points N of the electronic compass, and the vertical axis represents the calculated magnitude value $|B|$ based on the magnetic data. The magnitude values before and after calibration are displayed in red and blue, respectively. It is evident that the calibrated magnetic field magnitude fluctuates around a fixed value with a smaller range of variation compared to pre-calibration values, demonstrating that the error parameter calibration method successfully reduced manufacturing errors.

3.2. *Validation experiment for secondary compensation based on rotational stepping error fitting*

To verify the effectiveness of the proposed rotational stepping error fitting secondary compensation method, experiments were conducted on the electronic compass circuit board. The electronic compass circuit board was placed in a non-magnetic box that contained a fixed ARM controller and power supply battery. The box was secured to a base. The base comprised a stepping cylinder and a stepping base. The bottom of the stepping cylinder featured a 1° indented rack, while the stepping base contained a 1° protruding rack that interlocked with the indented rack of the stepping cylinder, thereby achieving 1° incremental rotation. The physical images of the stepping cylinder and stepping base are shown in Fig. 6, while the entire assembled apparatus is illustrated in Fig. 7. Upper computer software running on an external PC controlled the ARM controller, facilitating command transmission and data reception. To ensure experimental accuracy, the experiments were

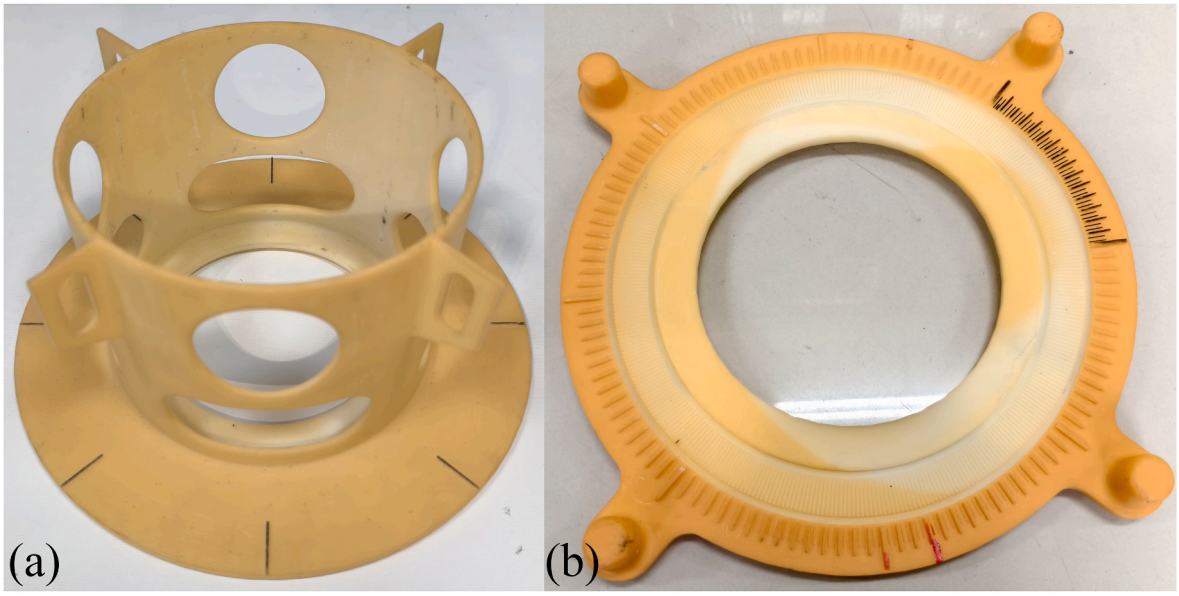

Fig. 6. Rotational stepping test platform. (a) Photograph of the stepping cylinder. (b) Photograph of the stepping base.

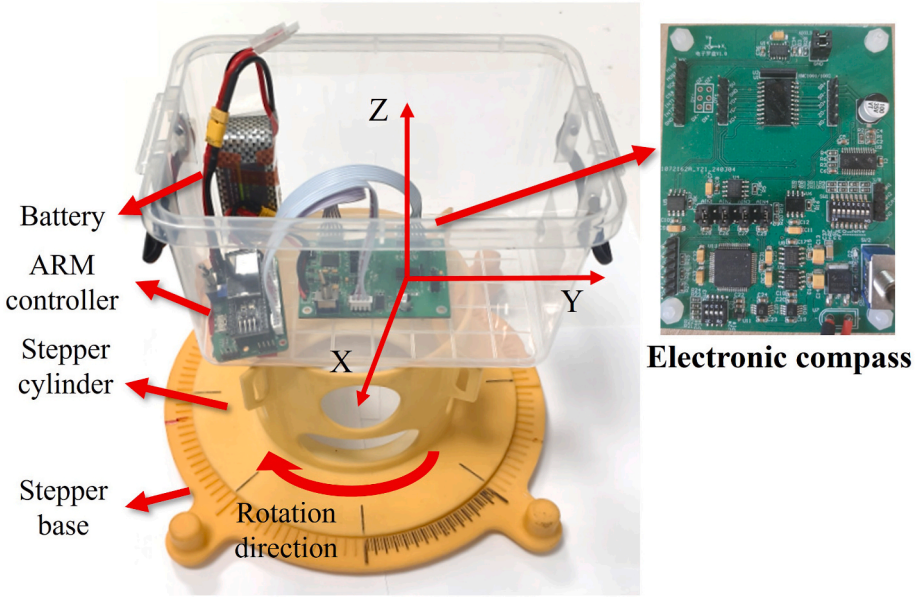

Fig. 7. Physical configuration of the electronic compass testing apparatus.

conducted in a stable, open area free from magnetic interference.

To validate the effectiveness of the proposed rotational stepping error fitting secondary compensation method under various magnetic disturbances, different ferromagnetic objects were fixed around the electronic compass to simulate diverse magnetic field interferences. Fig. 8 illustrates three different external magnetic disturbances simulated using magnetic iron pins.

Rotational stepping was performed according to the base scale gradations on the stepping base, and electronic compass data was collected. Three experiments were conducted with the interference configurations shown in Fig. 8. During the experimental process, the compass was rotated in 18° increments, with five sets of data collected at each step. The measured data was compared with the actual rotational azimuth angles, and the deviation between measured and actual angles was calculated.

Fig. 9 presents three sets of azimuth error results obtained from rotational stepping experiments under three different external magnetic field disturbances. The horizontal axis represents the actual azimuth angle ε, while the vertical axis represents the azimuth error δ calculated by the electronic compass. It is evident that significant errors exist in the measured azimuth angles after the ellipsoid fitting calibration of the electronic compass, with similar error patterns observed across the three different interference conditions. The errors were fitted, and the resulting curves based on the error data were plotted in Fig. 9, with the fitting results presented in Table 1. As evident from Fig. 9 and Table 1, the fitted curves accurately describe the variation trends of the three sets of azimuth error data.

The fitted compensation functions were utilized to perform compensation individually, yielding post-compensation azimuth errors. Fig. 10 illustrates the azimuth errors after compensation by the fitted

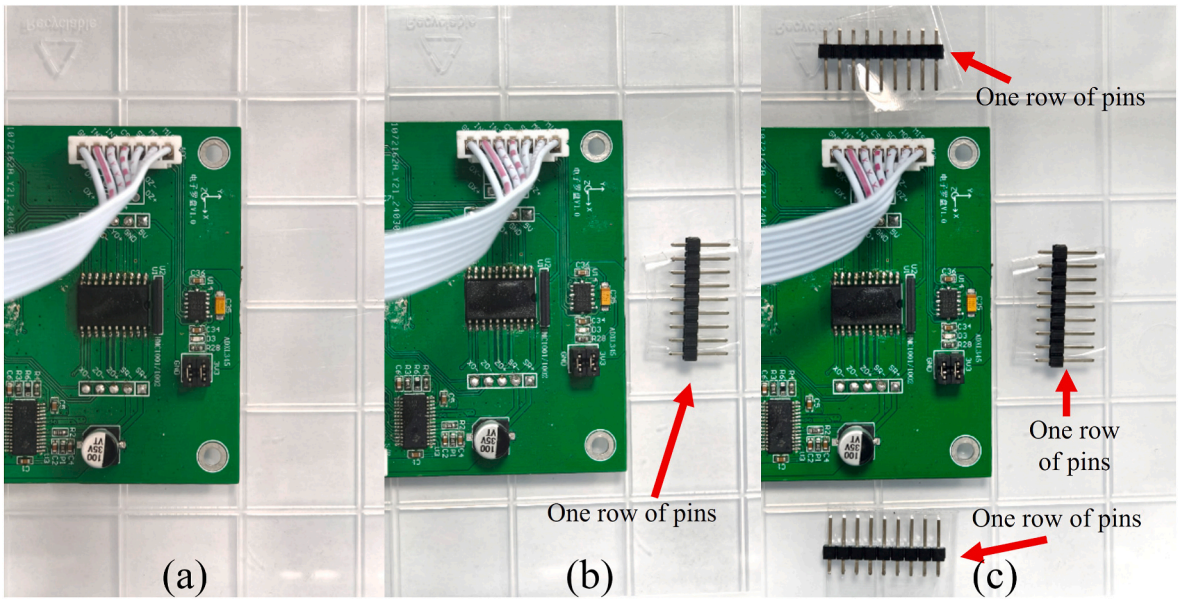

Fig. 8. External magnetic interference tests. (a) Type 1: with interference on compass only. (b) Type 2: with single row of ferromagnetic pins added. (c) Type 3: with three rows of ferromagnetic pins added.

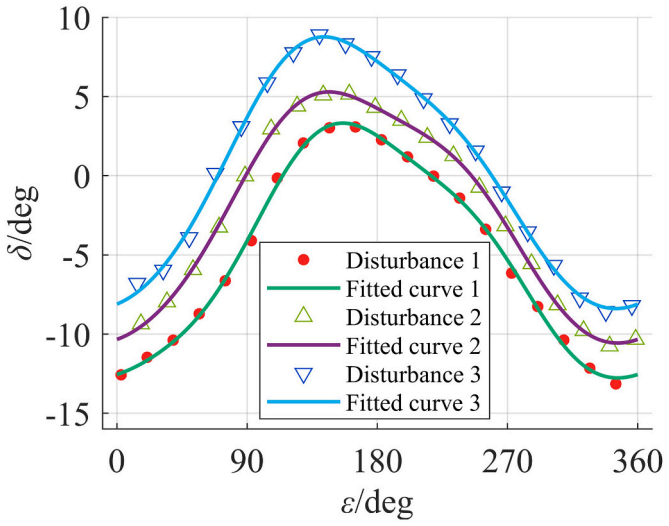

Fig. 9. Fitting curve of azimuth angle errors.

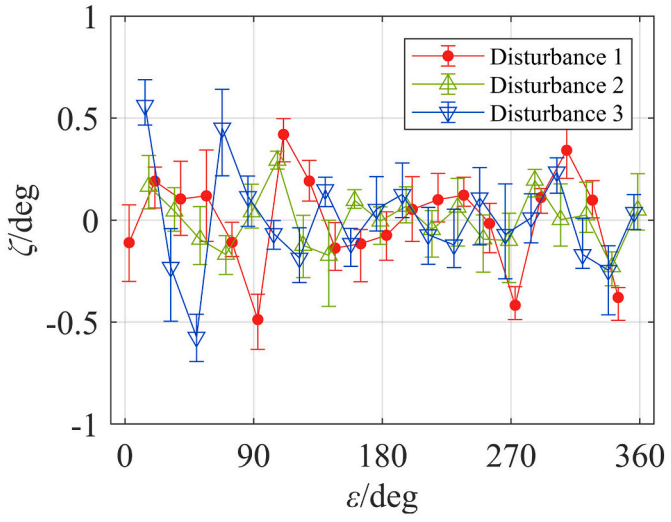

Fig. 10. Distribution of azimuth angle errors after compensation using the fitting function.

Table 1
Curve fitting results of Fig. 9.

Fitted coefficients	Fitted curve 1	Fitted curve 2	Fitted curve 3
A'	−4.8656	−2.2963	0.3134
B'	1.0795	1.8631	2.7003
C'	−7.8720	−7.6991	−8.0292
D'	−0.4193	−0.2268	−0.4227
E'	−0.1522	−0.7466	−0.7632
F'	0.4711	0.1435	0.0892
G'	0.3364	0.4082	0.3732
SSE	1.0582	0.3310	1.1917
MAE	0.1848	0.1035	0.1850
RMSE	0.2300	0.1286	0.2441
R^2	0.9983	0.9995	0.9984

functions, where the horizontal axis represents the actual azimuth angle ε, and the vertical axis represents the post-compensation azimuth error ζ. It can be observed that the azimuth error expression derived from the compensated azimuth errors effectively reflects the electronic compass azimuth errors.

4. Azimuth measurement experiment of the buoy

4.1. Design of experiment

To validate the proposed rotational stepping error fitting compensation method on buoys, we designed an experimental apparatus simulating buoy operation, as shown in Fig. 11. This apparatus consisted of a sleeve, stepping cylinder, stepping base, electronic compass, and ARM controller. The setup included a 3D-printed cylindrical sleeve (18

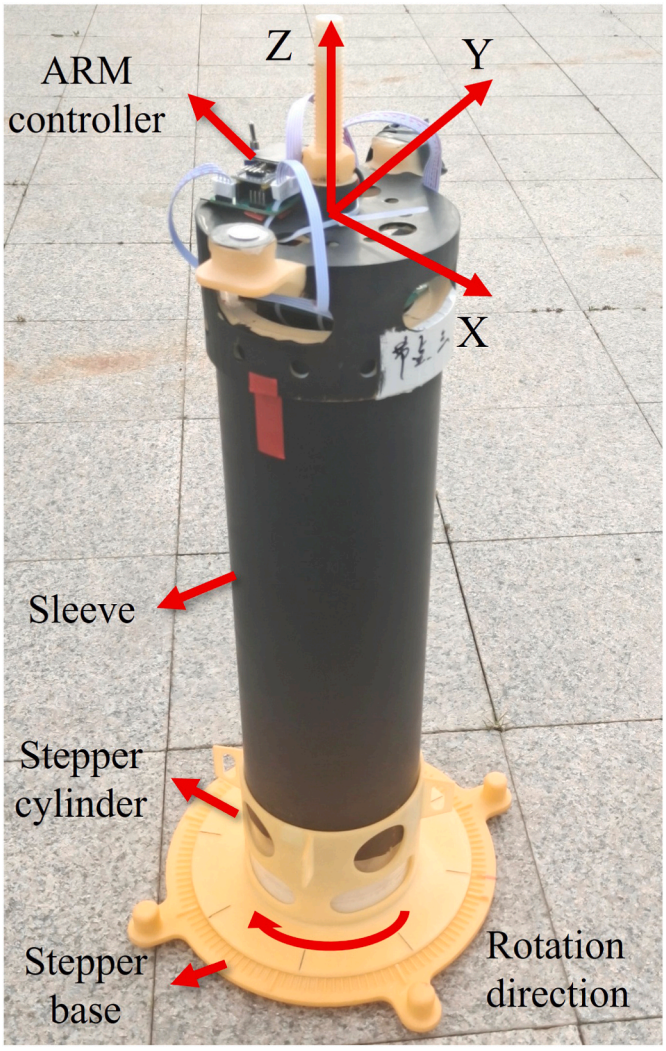

Fig. 11. Photograph of the azimuth rotational stepping test apparatus.

cm diameter, 60 cm height) to replicate the buoy structure, along with the stepping cylinder and base described in Section 3. The electronic compass, designed as detailed in Section 3 and pre-calibrated using ellipsoidal fitting, was installed in the sleeve alongside the ARM controller. An external PC running upper computer software managed command transmission and data collection.

4.2. Analysis of experimental results

Experiments were conducted using the fabricated buoy rotational stepping apparatus. During the rotational stepping experiments, the sleeve with the stepping cylinder was positioned on the stepping base, ensuring precise engagement between the cylinder and the rack on the base. The rotation procedure involved 9-degree incremental steps, with five sets of data collected at each position. The measured data were compared with the actual azimuth angles, and the deviations between them were calculated, with results shown in Fig. 12(a).

Fig. 12(a) presents the azimuth error fitting graph, where the x-axis represents the actual azimuth ε and the y-axis represents the azimuth error δ. The azimuth compensation function derived from (28) effectively reflects the azimuth error patterns of the buoy. The fitted compensation function was applied to correct the azimuth measurements, with the resulting errors shown in Fig. 12(b), where the x-axis represents the actual azimuth ε and the y-axis represents the compensated azimuth error ζ. The compensated electronic compass error was observed to be less than 0.4°, demonstrating that the rotational stepping error fitting two-step compensation method effectively reduces azimuth

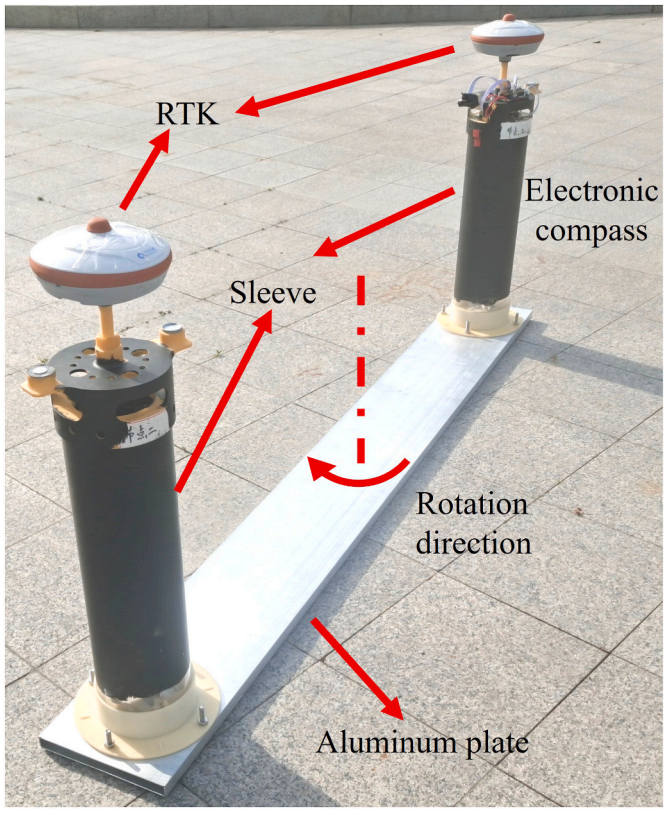

Fig. 13. Comparison test apparatus for azimuth measurement accuracy.

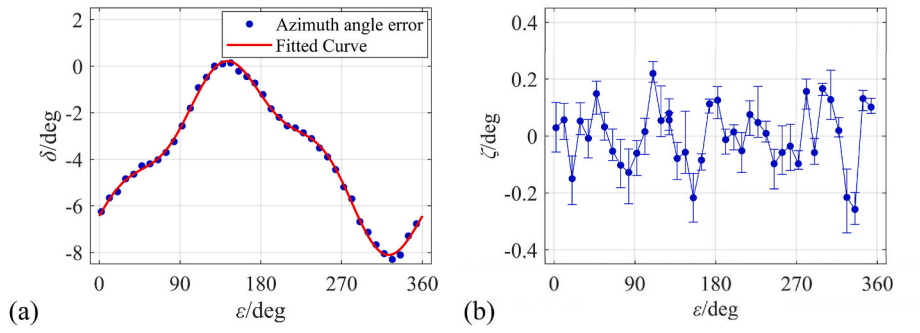

Fig. 12. Results of rotational stepping compensation test: (a) azimuth error fitting graph. (b) distribution of azimuth errors after compensation using the fitted function.

measurement errors in electronic compasses.

4.3. Precision validation experiment for buoy azimuth measure

To validate the accuracy of the proposed rotational stepping error fitting secondary compensation method, an absolute azimuth verification apparatus was designed based on the rotational stepping experiments. The experimental apparatus, as shown in Fig. 13, consisted of an aluminum plate, two high-precision satellite positioning devices, two identically-sized sleeves, and a PC. Two sleeves were mounted at each end of the aluminum plate, with each sleeve supporting one positioning device. The aluminum plate, measuring 1.73 m in length, was utilized to maintain a constant relative position between the two positioning devices. Mounting holes for the sleeves were positioned at both ends of the plate, establishing a fixed distance of 1.5 m between the sleeves. The high-precision satellite positioning device employed was Qianxun SE-Lite, capable of achieving 2 cm positioning accuracy. Of the two identical sleeves, one housed both a three-dimensional electronic compass and a high-precision satellite positioning device, while the other contained only a high-precision satellite positioning device. This configuration ensured consistent heights for the satellite positioning devices. The overall azimuth measurement accuracy of the apparatus was 0.76°.

The experimental environment required an open area free from electronic device interference to ensure high-quality reception of satellite positioning signals. The geographic north-south direction was determined based on the latitude and longitude information output by the two positioning devices, and the azimuth angle φ' from the electronic compass was recorded. The absolute azimuth of the apparatus was calculated using positioning data from the two devices in the absolute azimuth verification apparatus. The effective azimuth output from the compensated electronic compass was recorded as the measured value of absolute azimuth, with the difference between these values representing the measurement error of the absolute azimuth. As illustrated in Fig. 13, the apparatus rotated around the vertical centerline of the aluminum plate.

During the validation process, the aluminum plate was rotated approximately 20° for each measurement. Twenty sets of three-dimensional electronic compass azimuth data were collected each time, with intervals of approximately 10 s between sets. The test results are presented in Fig. 14, where the x-axis in Fig. 14(a) represents the absolute azimuth Φ_a determined by the two positioning devices, and the y-axis represents the measured azimuth Φ_m of the compensated buoy. In Fig. 14(b), the x-axis represents the absolute azimuth Φ_a determined by the two positioning devices, while the y-axis represents the error ζ_m between the measured azimuth of the compensated buoy and the azimuth determined by the RTK positioning apparatus. As observed in Fig. 14(b), the maximum azimuth error was 0.551°, the minimum was −0.583°, and the average error was 0.0725°. Each data set exhibited a distribution range within 0.3°, indicating that the azimuth measurement accuracy was within 0.6°, demonstrating good precision.

Table 2
Azimuth measurement errors of electronic compasses using different calibration methods.

Calibration method	Maximum azimuth error
Uncalibrated	8.4°
Proposed method	0.6°
Helmholtz coil without sensor motion [13]	1°
Dual GPS absolute calibration [14]	0.64°
Ellipsoid method and 16-position method [20]	0.4°
Error-separation method and 6-postion method [25]	0.4°
EF-DPI-ORV [26]	0.24°

5. Method comparison and discussion

Table 2 presents the maximum azimuth measurement errors of electronic compasses calibrated using the proposed method and other methods. As demonstrated, the rotational stepping error fitting two-step compensation method proposed in this study reduced the maximum azimuth error from 8.4° (uncalibrated) to 0.6°, achieving superior azimuth measurement accuracy compared to the Helmholtz coil method and the dual satellite positioning method. Although higher calibration precision was achieved with the ellipsoid method and 16-position method, non-magnetic turntable method, and ellipsoid fitting-dot product invariant-optimal resultant vector (EF-DPI-ORV) three-step calibration method, these approaches required the use of non-magnetic turntables to collect electronic compass data at specified azimuth angles. These methods were primarily suitable for lightweight electronic compasses. Overall, the proposed method simplified external equipment requirements at the cost of some precision loss. This characteristic makes it more suitable for applications involving large-scale marine buoys that are difficult to rotate.

However, the proposed method still has several limitations: the correction accuracy performs better in applications with relatively stable buoy attitudes compared to scenarios involving dramatic attitude variations, making it unsuitable for buoys operating in extreme marine environments. Regarding interference resistance, the method demonstrates poor performance against external transient magnetic field interference, as instantaneous magnetic disturbances introduce additional noise that affects real-time azimuth measurements. The temperature drift and aging characteristics of sensors on the buoy affect the long-term stability of azimuth measurements. It should be noted that these limitations primarily stem from uncontrollable environmental factors, and in typical buoy azimuth measurement applications in open waters, the magnetic interference from the buoy platform itself remains the dominant source of systematic error.

To address these limitations, future research efforts will focus on enhancing the practical applicability of the method under real complex marine environments. This includes three key aspects. First, dynamic compensation will be integrated with attitude sensing to handle severe buoy motions. Second, transient magnetic field interference filtering mechanisms will be introduced to improve azimuth angle measurement

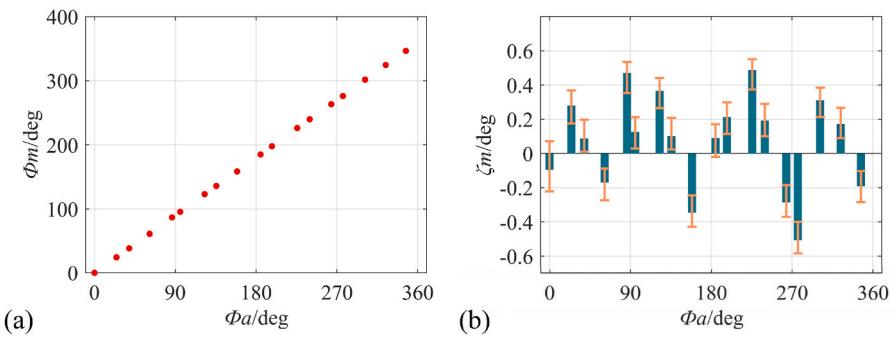

Fig. 14. Buoy azimuth accuracy validation results: (a) actual buoy azimuth measurement results; (b) distribution of actual buoy azimuth measurement errors.

reliability. Third, compensation models for sensor temperature drift and aging characteristics will be established, supplemented by in-situ micro-calibration strategies to ensure long-term stability. Ultimately, long-term sea-based mounting tests will be conducted on operational buoy platforms to comprehensively enhance the method's practicality.

6. Conclusion

In view of the characteristics of marine buoys having large volumes and complex internal magnetic interference, this paper proposes a joint two-step calibration scheme for buoy electronic compasses, which avoids the use of three-dimensional rotation operations and large Helmholtz coils. In the first step of this method, before installation in the buoy, the electronic compass magnetometer undergoes initial calibration using the ellipsoid fitting method, requiring arbitrary rotation of the lightweight electronic compass around multiple different axes. The second step involves installing the electronic compass inside the buoy and performing rotational stepping secondary compensation to improve azimuth measurement accuracy. This step requires only one complete rotation of the buoy around the vertical axis, which is relatively easy to implement.

Initially, the working model of the electronic compass, conventional manufacturing error compensation model, and rotational stepping error fitting secondary compensation model were derived. Subsequently, an electronic compass was designed and subjected to ellipsoid fitting calibration, followed by secondary compensation tests under various soft magnetic interference conditions, validating the feasibility of the proposed rotational stepping error fitting compensation scheme. Experimental results demonstrate that the proposed azimuth error model accurately fits azimuth errors under different magnetic interferences, thereby enabling secondary compensation of azimuth errors.

Finally, the electronic compass was installed on a custom-designed buoy apparatus, and rotational stepping tests were conducted with the buoy rotating around the vertical axis. The azimuth error data of the buoy electronic compass was collected, an error-azimuth function was fitted, and secondary compensation was completed. To further verify the measurement accuracy of the buoy azimuth, a pair of high-precision satellite positioning devices was utilized to measure the absolute azimuth of the buoy. Comparative tests were conducted on the azimuth measurement results of buoys that had undergone primary and secondary calibration. Results indicate that the azimuth error remained within 0.6°, confirming the feasibility and advantages of the rotational stepping secondary compensation proposed in this paper.

In conclusion, the joint two-step calibration scheme proposed in this study provides a high-precision, low-complexity approach for buoy azimuth measurement correction. Regarding the limitations identified in this work, future studies will conduct dynamic characteristic testing under actual operating conditions and introduce compensation mechanisms for sensor temperature drift to further improve the method's stability.

Credit author statement

Jinshuo Ma: Conceptualization, Methodology, Software, Writing - Original draft preparation. **Ningfeng Zhang:** Investigation, Data curation, Software, Writing - Review & Editing. **Tao Zhang:** Investigation, Visualization. **Jinyu Ma:** Supervision, Formal analysis. **Jian Li:** Project Administration, Validation. **Xinjing Huang:** Funding acquisition, Resources, Funding Acquisition, Writing - Review & Editing.

Declaration of competing interest

The authors declare that they have no known competing financial interests or personal relationships that could have appeared to influence the work reported in this paper.

Acknowledgments

This work is supported by National Natural Science Foundation of China (No. 62473279), Natural Science Foundation of Tianjin (No. 24JCZDJC01070), Tianjin National Key Laboratory Major Project (No. 24ZXZSSS00290), and Guangxi Key Laboratory of Automatic Detecting Technology and Instruments (No. YQ24203).

Data availability

Data will be made available on request.

References

[1] Zhizhong Lu, Xin Wu, Meng Linlin, Baotian Wen, An improved method to calculate principal wave direction from buoy data. 2019 4th International Conference on Control and Robotics Engineering (ICCRE), 2019, pp. 151–155.
[2] Zenghong Liu, Xu Jianping, Chaohui Sun, Xiaofen Wu, An upper ocean response to Typhoon Bolaven analyzed with Argo profiling floats, Acta Oceanol. Sin. 33 (2014) 90–101.
[3] Nandakumaran Nadarajah, Jens-André Paffenholz, Peter J.G. Teunissen, Integrated GNSS attitude determination and positioning for direct geo-referencing, Sensors 14 (7) (2014) 12715–12734.
[4] Pittorio M.N. Passaro, Antonello Cuccovillo, Lorenzo Vaiani, Martino De Carlo, Carlo Edoardo Campanella, Gyroscope technology and applications: a review in the industrial perspective, Sensors 17 (10) (2017) 2284.
[5] Surui Xie, et al., Seafloor geodesy in shallow water with GPS on an anchored spar buoy, J. Geophys. Res. Solid Earth 124 (11) (2019) 12116–12140.
[6] Aamir Rashid, Syed Shah, Abdul Rehman, Calibration of flux gate compass for underwater applications. 2016 International Conference on Open Source Systems & Technologies (ICOSST), 2016, pp. 1–6.
[7] Hongfeng Pang, et al., Calibration of three-Axis fluxgate magnetometers with nonlinear least square method, Measurement 46 (4) (2013) 1600–1606.
[8] R. Markovič, A. Krajnc, D. Matko, Calibration of a solid-state magnetic compass using angular-rate information from low-cost sensors, IET Sci. Meas. Technol. 5 (2) (2011) 54–58.
[9] Maoran Zhu, Yuanxin Wu, Wenxian Yu, An efficient method for gyroscope-aided full magnetometer calibration, IEEE Sens. J. 19 (15) (2019) 6355–6361.
[10] D.-X. Chen, High-field ac susceptometer using Helmholtz coils as a magnetizer, Meas. Sci. Technol. 15 (6) (2004) 1195.
[11] Torben Risbo, et al., Ørsted pre-flight magnetometer calibration mission, Meas. Sci. Technol. 14 (5) (2003) 674.
[12] Zhongyan Liu, Zhang Qi, Mengchun Pan, Qingxiao Shan, Yunling Geng, Guan Feng, Distortion magnetic field compensation of geomagnetic vector measurement system using a 3-D Helmholtz coil, IEEE Geosci. Rem. Sens. Lett. 14 (1) (2016) 48–51.
[13] Tommaso Lapucci, Luigi Troiano, Carlo Carobbi, Lorenzo Capineri, Soft and hard iron compensation for the compasses of an operational towed hydrophone array without sensor motion by a Helmholtz coil, Sensors 21 (23) (2021) 8104.
[14] Marc Le Menn, Michel Le Goff, A method for absolute calibration of compasses, Meas. Sci. Technol. 18 (5) (2007) 1614.
[15] Marc Le Menn, et al., Current profilers and current meters: compass and tilt sensors errors and calibration, Meas. Sci. Technol. 25 (8) (2014) 085801.
[16] Valérie Renaudin, Muhammad Haris Afzal, Gérard Lachapelle, Complete triaxis magnetometer calibration in the magnetic domain, J. Sens. 2010 (1) (2010) 967245.
[17] Zhicheng Yang, Li Bin, Lianping Chen, Calibration of tri-axis magnetometers using an improved truncated singular value decomposition method, Meas. Sci. Technol. 29 (12) (2018) 125101.
[18] Maryam Kiani, Seid H. Pourtakdoust, Sheikhy Ali Akbar, Consistent calibration of magnetometers for nonlinear attitude determination, Measurement 73 (2015) 180–190.
[19] Long Dafeng, Xiaoming Zhang, Wei Xiaohui, Zhongliang Luo, Jianzhong Cao, A fast calibration and compensation method for magnetometers in strap-down spinning projectiles, Sensors 18 (12) (2018) 4157.
[20] Jiancheng Fang, Hongwei Sun, Juanjuan Cao, Zhang Xiao, Tao Ye, A novel calibration method of magnetic compass based on ellipsoid fitting, IEEE Trans. Instrum. Meas. 60 (6) (2011) 2053–2061.
[21] Xiaoming Zhang, Guobin Chen, Li Jie, Jun Liu, Calibration of triaxial MEMS vector field measurement system, IET Sci. Meas. Technol. 8 (6) (2014) 601–609.
[22] Yanxia Liu, Li Xisheng, Feng Yibo, Xiaojuan Zhang, Research on calibration position distribution of three-axis magnetic compass, Chin. J. Sci. Instrum. 34 (3) (2013) 684–690.
[23] Marc Le Menn, Dominique Lefevre, Katrin Schroeder, Mireno Borghini, Study of the origin and correction of compass measurement errors in Doppler current meters, Front. Mar. Sci. 10 (2023) 1254581.
[24] W. Denne, Magnetic Compass Deviation and Correction, third ed., Brown Son Fergusson, 1998, p. 165.
[25] Zhiwei Chu, Xinhua Lin, Ke Gao, Chilai Chen, Error-separation method for the calibration of magnetic compass, Sensor Actuator Phys. 250 (2016) 195–201.

[26] Xiaoning Zhu, Zhao Ta, Defu Cheng, Zhijian Zhou, A three-step calibration method for tri-axial field sensors in a 3D magnetic digital compass, Meas. Sci. Technol. 28 (5) (2017) 055106.
[27] Zongwei Liu, Lei Kan, Jiancheng Song, Li Linbo, Li Tao, A designed calibration approach for the measurement-while-drilling instrument, Appl. Sci. 13 (1) (2022) 61.
[28] Ruoyin Wang, Xueliang Huang, Multi-degree of freedom accurate offset angle measurement for coils based on 3D electronic compasses, IEEE Sens. J. 21 (19) (2021) 22038–22046.
[29] Jean Metge, et al., Calibration of an inertial-magnetic measurement unit without external equipment, in the presence of dynamic magnetic disturbances, Meas. Sci. Technol. 25 (12) (2014) 125106.
[30] N. Grammalidis, M.G. Strintzis, Head detection and tracking by 2-D and 3-D ellipsoid fitting. Proceedings Computer Graphics International, 2000, 2000, pp. 221–226.
[31] Andrew Fitzgibbon, Maurizio Pilu, Robert B. Fisher, Direct least square fitting of ellipses, IEEE Trans. Pattern Anal. Mach. Intell. 21 (5) (1999) 476–480.
[32] Li Xiang, Li Zhi, A new calibration method for tri-axial field sensors in strap-down navigation systems, Meas. Sci. Technol. 23 (10) (2012) 105105.
[33] Zhitian Wu, Xiaoping Hu, Meiping Wu, Juliang Cao, Constrained total least-squares calibration of three-axis magnetometer for vehicular applications, Meas. Sci. Technol. 24 (9) (2013) 095003.
[34] Yaxin Mu, Luzhao Chen, Xiao Yao, Small signal magnetic compensation method for UAV-borne vector magnetometer system, IEEE Trans. Instrum. Meas. 72 (2023) 1–7.